Mixing in an agitated tubular reactor

J.J. Derksen

School of Engineering, University of Aberdeen, Aberdeen, UK

jderksen@abdn.ac.uk

Submitted to Special Issue WCCE10/CFD of CJCE – January 2018

Revision submitted February 2018

Abstract

We analyze, through numerical simulations, the single-phase liquid flow and associated passive scalar mixing in a tubular reactor that is agitated by lateral shaking which induces the motion of a solid mixing element inside the reactor. The Reynolds number associated to the shaking motion is in the range 1,200 – 5,600. Dependent on its specific value we perform direct or large-eddy simulations. A fixed-grid lattice-Boltzmann method is used for solving the fluid flow. The moving boundary condition at the surface of the mixing element is dealt with by means of an immersed boundary method. To quantify mixing, a transport equation for a passive scalar is solved in conjunction with the flow dynamics.

Keywords

Tubular reactor, mixing, direct & large-eddy simulation, immersed boundary method, scalar transport

1 Introduction

A novel type of continuous mixing system is shown in Figure 1. It consists of an outer tube with circular cross section that undergoes a sinusoidal motion in the lateral horizontal direction. This – in turn – induces the lateral motion and rotation of a solid internal mixing element (called "the internal" in the remainder of this paper) that has the form of a round tube with holes, as depicted in the figure. This through-flow mixing system can be used as a reactor, a blender, as well as a system to promote solid particle suspension and agitation. In this paper we only consider its single-phase operation. The working fluid is a liquid of constant density and viscosity.

The research described in this paper is purely numerical and of an exploratory nature. The aim is to show the feasibility, as well as the limitations, of our numerical approach to solve fluid flow and scalar transport in this geometrically and kinematically complex flow system under transitional and mildly turbulent conditions. Such simulations then will allow us – in future work – to make predictions of the performance of this mixing device under specific process conditions that can be compared with experimental data as well as with the performance of other continuous flow mixing devices at comparable conditions.

As can be judged from Figure 1, the dimensionality of the parameter space of this mixing device is extensive and contains the frequency and amplitude of the shaking motion, liquid properties, the through-flow rate, gravitational acceleration and the density of the internal, as well as geometrical (i.e. aspect) ratios. Numerical simulations are an effective way to explore – for process design purposes – large parts of the parameter space and we plan to do so in future research. Future research also should involve the assessment of numerical effects – most importantly establishing grid independence – as well as validation by means of experimental data.

This brief paper is organized in the following manner: We will start by defining the flow system and characterizing it in terms of a set of dimensionless numbers. Then we make a number of simplifying assumptions. Subsequently turbulence treatment and numerical methods are briefly discussed, with

referencing to the literature for further details. In the Results section the first part describes flow field results, the second part passive scalar transport. The paper is closed with a Summary & Conclusions section.

2 Flow system

The geometrical layout of the agitated tubular reactor is given in Figure 1. The main geometrical parameters are the inner diameter of the outer tube (D) and its length L, as well as the diameter of the internal (D_i). Mixing is enhanced by holes in the cylindrical internal. The placement and diameters of the holes along with further details are provided in Figure 1 that also defines the coordinate system.

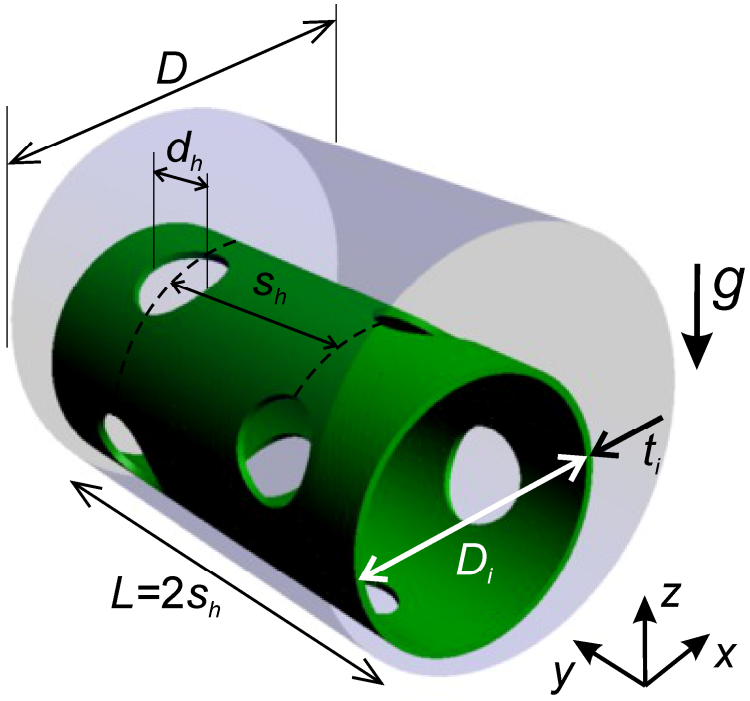

Figure 1. Flow geometry. An internal mixing element (in green) can move inside a tube of diameter D that is shaken in the x-direction. The internal feels a net gravity force that acts in the negative z-direction. The overall flow is in the y-direction; the simulations assume periodic conditions in y-direction. The dimensions as given in the drawing relative to the tube diameter are: $D_i = 0.62D$, $L = 1.28D$, $d_h = 0.25D$, $t_i = 0.013D$. The origin of the coordinate system is at the center of the outer tube and at its front.

The internal has three degrees of freedom, as specified in Figure 2. These are the lateral horizontal location of its center x_i, its vertical location z_i and its rotation angle α_i along the *y*-axis. The internal does not touch the outer tube with its surface. It has spacers that keep a minimum distance equal to ε between the inner surfaces of the outer tube and the outer surface of internal. The working fluid is Newtonian with kinematic viscosity ν and density ρ. The solid material the internal is made of has density $\rho_s = 8.0\rho$, except for one simulation that has a density ratio of 4.0. The internal feels a net gravity force in the negative *z*-direction.

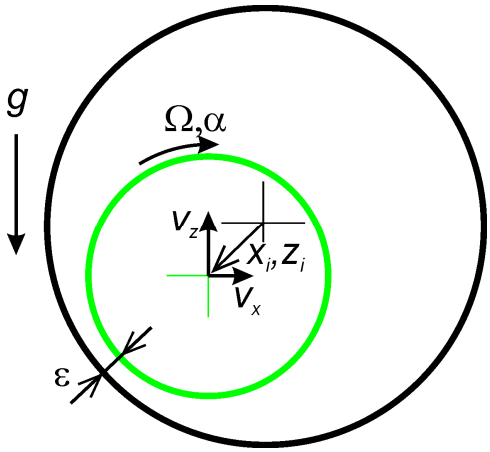

Figure 2. Schematic of the degrees of freedom of the internal (x_i, z_i and angle α), the associated velocities (v_x, v_z, Ω) and the minimum distance ε between internal and tube; $\varepsilon = 0.038D$.

The entire system is agitated by shaking it in a sinusoidal way in the *x*-direction: the displacement has amplitude *A* and frequency *f*: $A\sin(2\pi ft)$. This shaking induces motion of the internal which in turn induces mixing. When in operation, the mixer has a continuous through flow in the *y*-direction with volumetric flow rate ϕ_V giving rise to a superficial velocity of $U \equiv \frac{4\phi_V}{\pi D^2}$.

The above set of process parameters has been combined to a set of non-dimensional numbers where the length scale is mostly taken as the outer tube diameter *D*. Other dimensions of the system can be derived from the aspect ratios as given in Figures 1 and 2. The through-flow Reynolds number is defined

as $\mathrm{Re}_\phi \equiv \frac{UD}{\nu}$; the shaking motion is characterized by a Reynolds number $\mathrm{Re}_s \equiv \frac{2\pi fAD_i}{\nu}$, a Strouhal number $\mathrm{Str} \equiv \frac{fD}{U}$, and the amplitude over diameter ratio A/D. The ratio of shaking inertia and net gravity of the internal is expressed as $\theta \equiv \frac{\rho A(2\pi f)^2}{g(\rho_s - \rho)}$. Finally we have the density ratio ρ_s/ρ.

The simulations are performed in a reference frame that moves with the shaking motion. This implies that an inertial body force is applied to the liquid: $\mathbf{f} = -\rho A(2\pi f)^2 \sin(2\pi ft)\mathbf{e}_\mathbf{x}$. Furthermore we apply periodic conditions in the *y*-direction. This means that the geometry as shown in Figure 1 can be seen as a section taken from a much longer mixing system. A major simplification in the current study is that we set the volumetric flow rate $\phi_V = 0$. In this case, the mixing is only due to the shaking motion. It also implies that $\mathrm{Re}_\phi = 0$ and that the Strouhal number becomes infinite and, in this situation, is not a meaningful dimensionless parameter.

When the distance between the outer surface of the internal and the inner surface of the tube equals ε, the internal collides. In the simulations we have applied two collision models. In the hard model a fully elastic collision is performed and the velocity of the internal changes instantaneously. In the soft model, once the distance ε is reached, an elastic spring is activated that applies a normal repulsive force on the internal proportional to the overlap: $F_s = k(\varepsilon - s)$, with k the spring constant and $s < \varepsilon$ the distance between internal and outer tube. The hard as well as the soft model assume frictionless collisions so that the angular velocity Ω of the internal does not change upon collision.

3 Numerics

The lattice-Boltzmann method has been applied to solve the fluid flow. The specific numerical scheme is due to Somers [1]. The scheme applies a uniform, cubic (edge length Δ) grid with the flow variables defined in the cube centers. Off-grid boundary conditions, such as the no-slip conditions on the tube

surface and on the internal, are enforced through an immersed boundary method [2]. These surfaces are represented by a set of closely spaced points (nearest neighbor spacing typically 0.7Δ); for the internal this set of points is shown in Figure 3. At these points we force the fluid to have the same velocity as the local velocity of the solid surface. The immersed boundary method used is based on interpolation of velocities and extrapolation of forces [2]. Velocities at the immersed boundary points are estimated by interpolation of the surrounding grid velocities; the forces acting on the fluid at the immersed boundary points are extrapolated to the surrounding grid nodes. Integration of the immersed boundary forces over the surface of the internal gives the total hydrodynamic force $\mathbf{F}$ and torque $\mathbf{T}$ on the internal. The x and z component of $\mathbf{F}$ as well as the y component of $\mathbf{T}$ are taken into account when solving the equations of motion of the internal.

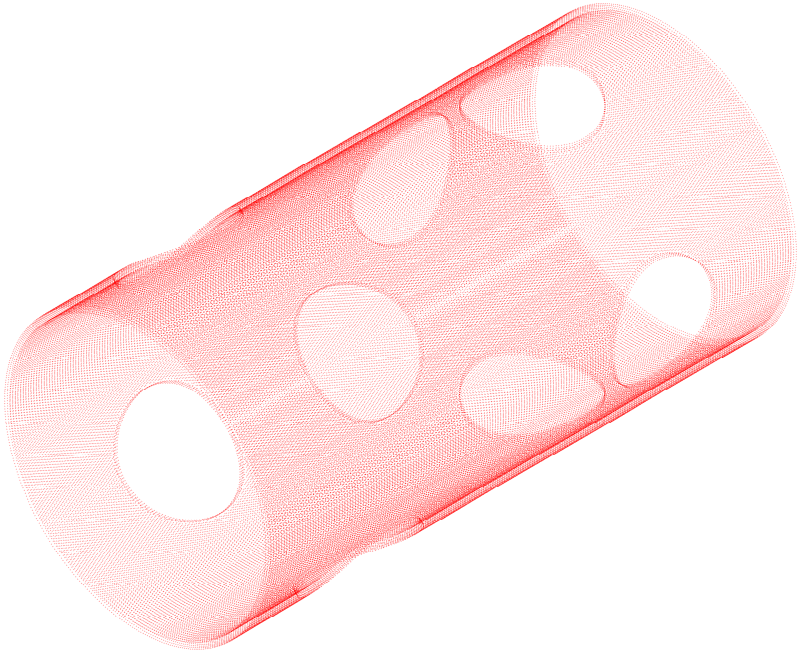

Figure 3. Representation of the internal mixing element by a closely spaced set of points on its surface. The total number of points is approximately 270,000.

In this study, the cubic grid has a resolution such that the tube diameter D spans 156 lattice spacings. This leads to an overall grid node count of approximately 5 million. The number of immersed boundary points on the internal is 270,000; on the outer tube it is 140,000. At this stage of the research we have not yet considered grid effects and thus are not able to show grid convergence. Time stepping in

lattice-Boltzmann methods is largely dictated by constraints on the Mach number [3]. In the simulations presented here, it takes 10,000 time steps to complete one shaking cycle, i.e. $f\Delta t = 1\cdot 10^{-4}$.

The three equations of motion of the internal (translational in *x* and *z* direction, rotational along the *y*-axis) are solved with a split-derivative method [4]. The forces on the internal are gravity and hydrodynamic force $\mathbf{F}$, as well as the collision force if a soft collision model is applied. The hydrodynamic torque $\mathbf{T}$ on the internal is included in the rotational equation of motion.

In addition to solving the flow and the dynamics of the internal, we have solved the transport of a passive scalar according to a convection-diffusion equation:

$$\frac{\partial c}{\partial t} + \mathbf{u}\cdot\nabla c = \Gamma\nabla^2 c \qquad (1)$$

with *c* the scalar concentration, $\mathbf{u}$ the velocity field that is the result of the lattice-Boltzmann flow solver, and Γ the diffusion coefficient. Equation 1 is discretized according to a finite volume method on the same (uniform, cubic) grid as applied by the lattice-Boltzmann scheme, and explicitly updated in time with the same time step as used in the lattice-Boltzmann method. We apply flux limiters [5] to suppress false diffusion. In the present work we set $\Gamma = 0$ so that the (limited) levels of diffusion observed in the simulations are due to the finite resolution of the grid and – still – some numerical diffusion. Procedures similar to the ones proposed in [6] were used for setting non-penetration boundary conditions at the moving solid surfaces of the internal, as well as for assigning scalar concentrations to grid nodes that are uncovered due to the motion of the internal.

In this work, the Reynolds numbers associated to the shaking motion (Re_s) were in the range 1,200 – 5,600. By default it was attempted to solve the flow without the use of a turbulence model. Unphysical instabilities occurred when Re_s exceeded approximately 3,000. In such situations we switch to large-eddy simulations (LES) and apply a standard Smagorinsky subgrid scale model [7] with Smagorinsky constant $C_S = 0.1$. In the LES cases, the scalar diffusion coefficient Γ is kept at zero level, i.e. we do not apply a finite level turbulent Schmidt number.

4 Results

4.1 Fluid flow

A base case has been defined with the following dimensionless parameters: Re_s =5,600, A/D =1.13, ρ_s/ρ =8.0, and $\theta = 0.37$ and the geometry as defined in Figures 1 and 2. This case applies hard collisions between internal and outer tube, and a large-eddy approach for turbulence modelling. In Figure 4 impressions of the flow field in a *xz*-cross section passing through four holes in the internal ($y = L/4$). The shaking motion is started with the internal in the centre of the outer tube ($x_i = z_i = 0$) and fluid at rest ($\mathbf{u} = \mathbf{0}$ everywhere). The velocity magnitude contour plots in Figure 4 illustrate how the flow develops from this initial condition. These – and all subsequent – images are in the reference frame moving with the shaking motion. Initially ($t = 0.25/f$) the internal moves down due to net gravity and to the right since the shaking motion starts to the left. In the subsequent frames we see an overall increase in the velocity magnitude. The velocity vector plot shows an instantaneous flow field after the system has fully developed. It also gives an impression of the level of resolution of the simulations.

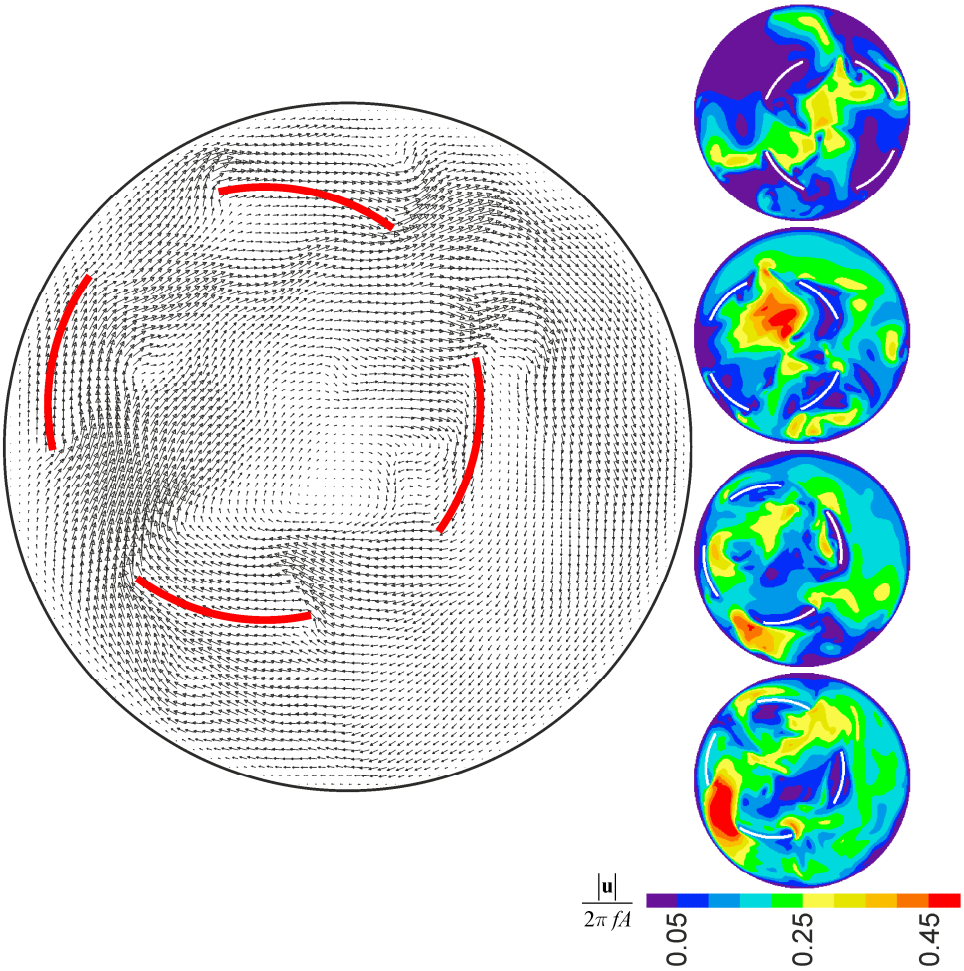

Figure 4. Left: instantaneous velocity vectors in an *xz* cross section of the flow at $y = L/4$ after the flow is fully developed. Right: impressions of how the flow starts in terms of velocity magnitude contours in the same *xz*-plane. From top to bottom: $tf = 0.25, 0.5, 1.0, 2.0$. Base-case conditions.

Under base-case conditions, the motion of the internal quickly settles in a periodic state, as can be judged from the time series of the vertical (center) location of the internal in Figure 5. For an effective operation of this mixing device, inertia of the internal appears important. If we change the density ratio from ρ_s/ρ=8.0 (base-case) to 4.0 and keep all other parameters the same, the internal gets hardly agitated (see the 2nd time series in Figure 5) which has detrimental effects on the mixing performance.

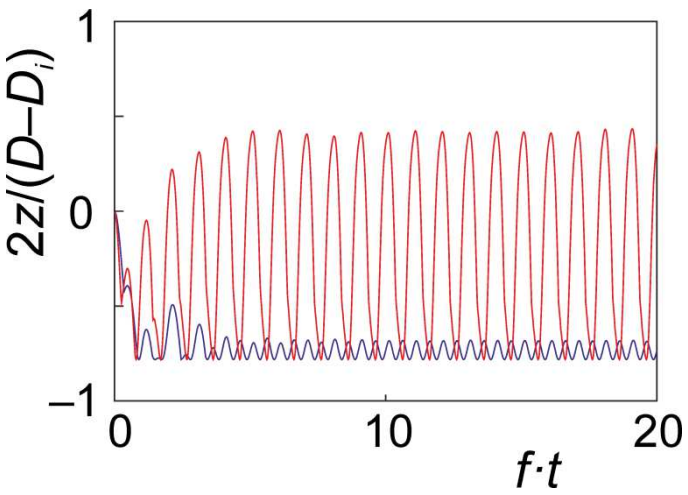

Figure 5. Time series of the vertical (z) coordinate of the center location of the internal. Red curve: base-case (which has a density ratio ρ_s/ρ=8.0); blue curve: same as base-case except that ρ_s/ρ=4.0.

At Re_s=2,300 we are able to get stable results without the use of a subgrid-scale model. If we compare these "direct" simulation results with ones obtained with a Smagorinsky subgrid-scale model at the same Reynolds number we see hardly any difference in the flow field as well as in the levels of agitation of the internal. As an illustration we show, in Figure 6, very close agreement of the time series of the vertical position of the internal as obtained with LES and DNS. These results imply that our procedure is able to represent in a smooth way the transition from laminar to turbulent flow.

Modelling the collisions of the internal is an important aspect of the simulations. In the hard collision model the velocity of the internal changes instantaneously at the moment of the collision. Given the slightly compressible nature of the lattice-Boltzmann scheme [3] this generates waves in the fluid. These waves are unphysical if the intention is to simulate an incompressible flow. The waves can be avoided by making the collisions "soft" and using an elastic spring that generates a repulsive force on the internal to push it away from the outer wall. The choice of collision model has some impact on the motion of the internal as can be seen in Figure 7. The soft model leads to some vibrations of the internal. On average, however, the soft and hard model result in very similar motion of the internal. Without any benchmark or experimental data it is hard to judge which collision model gives more reliable results. In

the remainder of this paper – when discussing scalar transport – results have been generated by using the hard model.

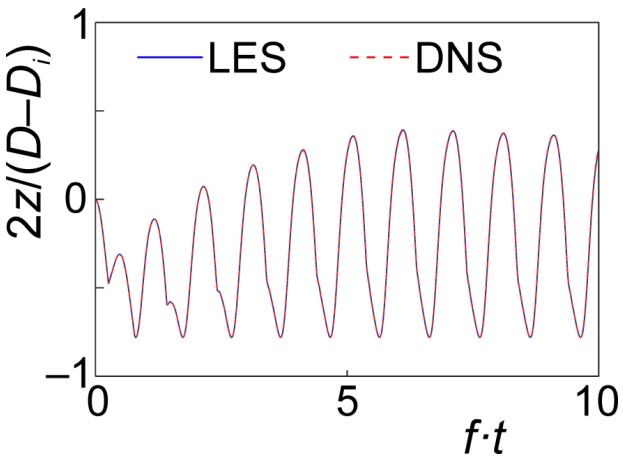

Figure 6. Time series of the vertical (z) coordinate of the center location of the internal. Comparison between LES and DNS at Re_s =2,300. The rest of the conditions are the same as for the base-case.

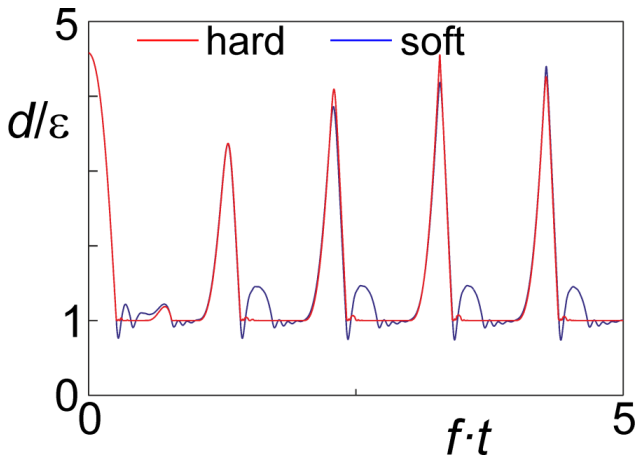

Figure 7. Time series reflecting the differences as a result of collision modelling; hard versus soft collisions. The parameter d is the distance of the internal from the wall so that a collision takes place if $d/\varepsilon = 1$. Base-case conditions except that Re_s =2,300. DNS flow simulations.

4.2 Passive scalar transport

In order to directly test the mixing performance of the agitated tubular reactor, the transport equation of a passive scalar concentration c (Eq. 1) was solved in conjunction with the flow dynamics. The initial condition for the simulations involving scalar transport is a fully developed flow field and a segregated scalar concentration field. The latter means that we set $c = 1$ for $z > 0$, and $c = 0$ for $z < 0$.

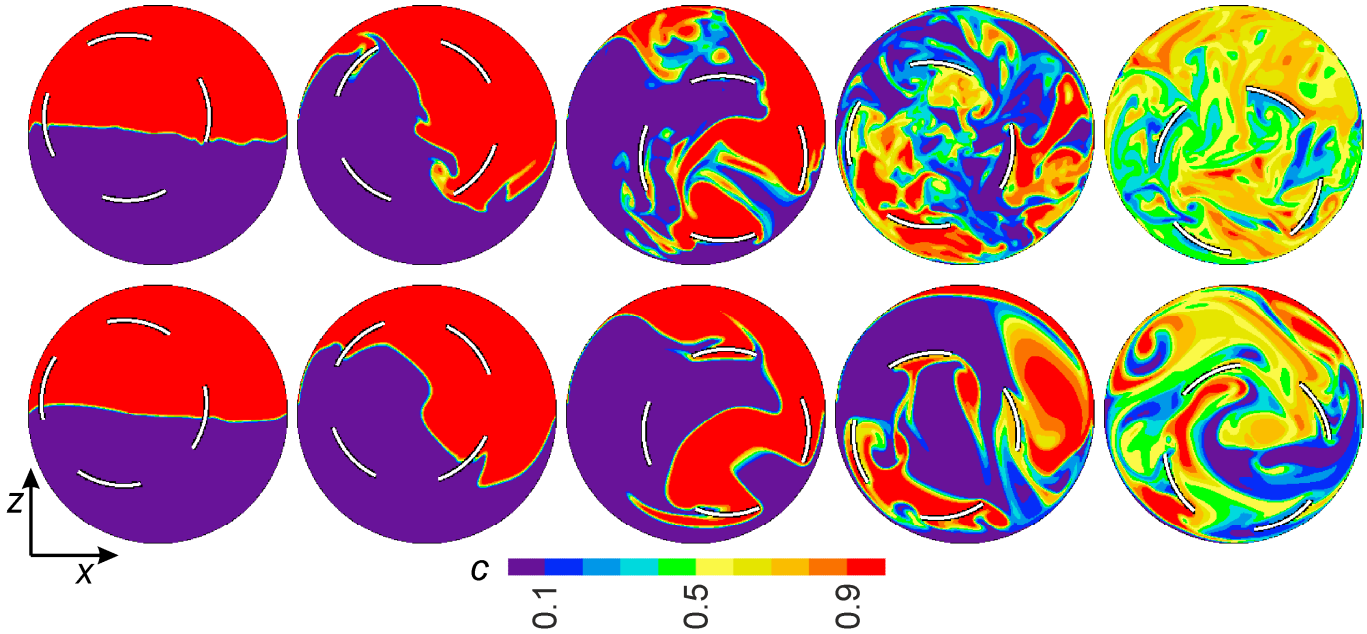

Figure 8. Scalar mixing in the form of concentration contours in the *xz*-plane at $y = L/4$. Top row: Re_s =5,600 (LES); bottom row: Re_s =1,200 (DNS). From left to right $tf = 0.02, 0.2, 0.4, 0.8, 1.6$ with at $t = 0$ a fully developed flow and a segregated scalar field.

In Figure 8 impressions of the mixing process are shown for two different Reynolds numbers Re_s. We see the formation of scalar concentration striations and – in the course of time – a homogenization of the concentration field with faster mixing for the higher Reynolds number. To quantify mixing we define the scalar variance as $\sigma_c \equiv \sqrt{\langle c^2 \rangle - \langle c \rangle^2} \,/ \langle c \rangle$ with $\langle\ \rangle$ denoting spatial averaging over instantaneous realizations of the concentration field, so that σ_c is a function of time. In Figure 9 we show an example of a σ_c time series where the spatial average is taken over the center vertical (*yz*) plane. Given that at time zero the scalar is segregated, the starting value of σ_c is approximately $\frac{1}{2}\sqrt{2}$. We see the decay of scalar variance and it being faster for the higher Reynolds number. If $\sigma_c = 0.02$ is set as the level for a practically homogeneous system, then for Re_s =5,600 homogenization is achieved after less than 10 shaking periods; for Re_s =1,200 it takes at least 15 periods. The periodic fluctuations are due to the periodic motion of the internal.

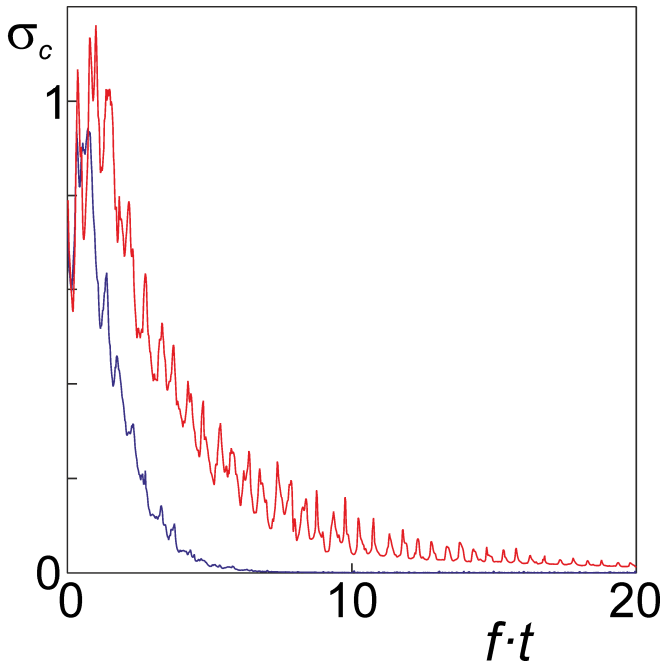

Figure 9. Time series of scalar variance $\sigma_c \equiv \sqrt{\langle c^2 \rangle - \langle c \rangle^2} \,/\, \langle c \rangle$ in the *yz*-plane with *x*=0 as a function of time for Re_s =5,600 (blue curve) and Re_s =1,200 (red curve).

5 Summary & conclusions

In this paper we have shown the feasibility of performing single-phase flow and mixing simulations of a novel agitated tubular reactor. Simulations so far have been on a systems operating in the transitional / early turbulent regime. It was shown that we can make a smooth transition from direct (i.e. no turbulence model) to large-eddy simulations. The simulation procedure is able to apply a hard as well as a soft model for the collisions of the internal mixing element with the outer tube wall. It was highlighted that the internal mixing element needs sufficient inertia (i.e. mass) to be sufficiently agitated by the shaking motion of the outer tube. Including passive scalar variance calculations allow for directly quantifying the mixing process, for instance in terms of the decay time of scalar variance.

This paper describes a feasibility study so that much more work needs to be done before applying the simulations for reactor design. The next steps are verification (e.g. establishing grid convergence) and validation (e.g. comparison with experimental data). Then we will be including through-flow so that we

will see mixing not only due to the motion of the internal but also due to an average axial velocity. It will be interesting to quantify the relative importance of these two contributions to mixing as a function of operational conditions.

Acknowledgement

Sincere thanks to Andrew Bayly and Yi He (University of Leeds, UK) for bringing this flow system to my attention.

References

[1] Somers, J.A., "Direct simulation of fluid flow with cellular automata and the lattice-Boltzmann equation," Appl. Sci. Res. 51, 127–133 (1993).

[2] Derksen, J. and H. E. A. Van den Akker, "Large-eddy simulations on the flow driven by a Rushton Turbine," AIChE J. 45, 209–221 (1999).

[3] Succi, S., "The lattice Boltzmann equation for fluid dynamics and beyond," Clarendon Press, Oxford (2001).

[4] Shardt, O. and J.J. Derksen, "Direct simulations of dense suspensions of non-spherical particles," Int. J. Multiphase Flow 47, 25–36 (2012).

[5] Sweby, P.K., "High resolution schemes using flux limiters for hyperbolic conservation laws," SIAM J. Numer. Anal. 21, 995–1011 (1984).

[6] Derksen, J.J., "Scalar mixing by granular particles," AIChE J. 54, 1741–1747 (2008).

[7] Smagorinsky, J., "General circulation experiments with the primitive equations: 1. The basic experiment," Mon. Weather Rev. 91, 99–164 (1963).